Development 137, 3707-3717 (2010) doi:10.1242/dev.052001

Frizzled 1 and frizzled 2 genes function in palate, ventricular septum and neural tube closure: general implications for tissue fusion processes

Huimin Yu[1], Philip M. Smallwood[1,2], Yanshu Wang[1,2], Roman Vidaltamayo[1,*], Randall Reed[1,3] and Jeremy Nathans[1,2,3,4,†]

SUMMARY

The closure of an open anatomical structure by the directed growth and fusion of two tissue masses is a recurrent theme in mammalian embryology, and this process plays an integral role in the development of the palate, ventricular septum, neural tube, urethra, diaphragm and eye. In mice, targeted mutations of the genes encoding frizzled 1 (Fz1) and frizzled 2 (Fz2) show that these highly homologous integral membrane receptors play an essential and partially redundant role in closure of the palate and ventricular septum, and in the correct positioning of the cardiac outflow tract. When combined with a mutant allele of the planar cell polarity gene *Vangl2* (*Vangl2*^{Lp}), *Fz1* and/or *Fz2* mutations also cause defects in neural tube closure and misorientation of inner ear sensory hair cells. These observations indicate that frizzled signaling is involved in diverse tissue closure processes, defects in which account for some of the most common congenital anomalies in humans.

KEY WORDS: Frizzled 1 (*Fz1; Fzd1*), Frizzled 2 (*Fz2; Fzd2*), Tissue closure, Mouse

INTRODUCTION

In the United States, more than 1% of infants born each year have a congenital anatomical anomaly (colloquially referred to as a 'birth defect') (Centers for Disease Control, 1997; New York State Department of Health, 2001). Among the most common anomalies are defects in positioning of the cardiac outflow tract and in closing of the ventricular septum, palate or neural tube; these occur at frequencies of ~0.2%, ~0.4%, ~0.1% and ~0.1% of live births, respectively (Genisca et al., 2009; Hoffman and Kaplan, 2002). Although these defects are found most commonly in isolation, they are also observed as components of a large number of syndromes that feature multiple congenital anomalies, and they are more common in embryos that have undergone spontaneous abortion (Shepard et al., 1989). In both humans and mice, the genetic contributions to these processes are complex (Copp and Greene, 2010; Jugessur and Murray, 2005; Juriloff and Harris, 2008; Kibar et al., 2007a; Moon, 2008).

One of the principal signaling systems implicated in embryonic patterning is tissue/planar cell polarity (PCP), a non-canonical Wnt signaling pathway (Veeman et al., 2003). PCP functions in diverse contexts to coordinate cell shape, movement and polarity within the plane of an epithelial sheet. Core vertebrate PCP genes include homologs of the *Drosophila* genes *frizzled* (*Fz3* and *Fz6*), *Van Gogh* (*Vangl1* and *Vangl2*), *dishevelled* (*Dvl1-3*) and *starry night* (*Celsr1-3*) (Seifert and Mlodzik, 2007; Wang and Nathans, 2007). In vertebrates, PCP genes are required for convergent extension, a process in which cells within an epithelial sheet rearrange in a coordinated manner to produce a narrowing of the tissue along one axis and an extension along the orthogonal axis. In neural tube closure, these movements lead to the progressive narrowing of the folding neural plate (Keller, 2002; Wallingford et al., 2002). In mice, PCP gene mutations produce defects in neural tube and eyelid closure, elongation of the cochlea and orientation of hair follicles in the skin and of sensory hair bundles in the inner ear (Wang and Nathans, 2007). Murine PCP gene mutations also produce a variety of cardiac anomalies, most commonly outflow tract and ventricular septal defects (Henderson et al., 2006; Henderson et al., 2009). In humans, mutations in *VANGL1* have been associated with neural tube defects (Kibar et al., 2009; Kibar et al., 2007b). There is also an essential role for canonical Wnt signaling in the closure of the neural tube, palate, ventricular septum and ventral fissure of the eye, based on the phenotype of LDL-receptor related protein 6 (*Lrp6*) mutant mice (Pinson et al., 2000; Song et al., 2009; Song et al., 2010). It is not known whether this dependence on the canonical Wnt pathway principally reflects a requirement for rapid cell proliferation.

Among the ten mammalian frizzled (Fz or Fzd) proteins, Fz3, Fz5 and Fz6 have thus far been implicated in tissue closure. *Fz5*$^{-/-}$ mice exhibit coloboma (failure to close the ventral fissure of the eye) (Liu and Nathans, 2008) and *Fz3*$^{-/-}$;*Fz6*$^{-/-}$ mice exhibit craniorachischisis (a fully open neural tube), a partially penetrant failure of eyelid closure, and misorientated auditory and vestibular sensory hair cells (Wang et al., 2006). Prior to the present work, mammalian frizzled gene mutations had not been associated with defects in palate or cardiac development, and it was not known whether frizzled genes other than *Fz3* and *Fz6* contribute to neural tube closure or inner ear development.

In this paper, we describe the production of mice with targeted mutations in *Fz1* and *Fz2*, and the observation that these genes function redundantly in the positioning of the cardiac outflow tract, in closure of the ventricular septum and in palate closure. We also show that *Fz1* and *Fz2* interact genetically with the *loop-tail* allele

[1]Department of Molecular Biology and Genetics, [2]Howard Hughes Medical Institute, [3]Department of Neuroscience, [4]Department of Ophthalmology, Johns Hopkins University School of Medicine, Baltimore, MA 21205, USA.

*Present address: Universidad de Monterrey, Department of Basic Science, Monterrey, NL 66238, Mexico
†Author for correspondence (jnathans@jhmi.edu)

Accepted 31 August 2010

of *Vangl2* (*Vangl2*^{Lp}) in neural tube closure and that *Fz2* plays a role in the orientation and organization of sensory hair cells in the cochlea.

MATERIALS AND METHODS

Generation of *Fz1* and *Fz2* mutant mice

The *Fz1* and *Fz2* targeting constructs carry the coding region of a nuclear-localized β-galactosidase (β-gal) in place of the frizzled coding region (the nuclear localization signal sequence, MGPKKKRKVGS, is at the N-terminus of β-gal), a *loxP*-flanked *PGK-neo* gene for positive selection and *HSV-TK* gene for negative selection. *Fz1* and *Fz2* constructs were electroporated into Sv129 (R1) ES cells and plated in G418 and ganciclovir. Colonies were screened by Southern blotting, and clones carrying the targeted allele were injected into C57BL/6 blastocysts. Chimeras were bred to C57BL/6, and the *loxP*-flanked *PGK-neo* cassette was removed with germline *Sox2-Cre* (Hayashi et al., 2002) [*Tg(Sox2-Cre)1Amc/J*, Jackson Laboratories]. Targeted *Fz1* and *Fz2* alleles were maintained both on a mixed C57BL/6 × Sv129 background and on a pure Sv129 background. PCR primers for the endogenous *Fz1* gene are 5′-TATGTGTATGTGCGTGTGGACCG-3′ and 5′-AAGGAAATGAC-CCTGGAGAGGCAG-3′. Primers for the knock-in *Fz1 lacZ* allele are 5′-CTGGACCACTCTTGCTCTCCTCG-3′ and 5′-TGGGATAGGTTAC-GTTGGTGTAGATG-3′. For *Fz2* genotyping, three primers were used: a shared sense primer (5′-GCACAAAGGAGTCGCTGGGTAGAG-3′), an antisense primer in the endogenous *Fz2* coding region that is deleted in the targeted allele (5′-GCGTCTCCTTGCAAACTTTGCTC-3′) and an antisense primer in the knock-in *lacZ* allele (5′-TGGGATAGG-TTACGTTGGTGTAGATG-3′).

Vangl2^{Lp} mice

Vangl2$^{Lp/+}$ mice were purchased from Jackson Laboratories. Genotyping primers were 5′-GACCCACCATCCAGTACCAC-3′ and 5′-CGCAT-GACGAACTTATGTG-3′. The PCR product was sequenced to reveal the sequence for the wild type and/or the *Vangl2*^{Lp} missense mutation (Kibar et al., 2001; Murdoch et al., 2001).

Histology and immunohistochemistry

Embryos from timed matings were dissected in ice-cold PBS, fixed overnight in 4% paraformaldehyde (PFA) in PBS at 4°C, dehydrated, embedded in paraffin and sectioned at 7 μm. Hematoxylin and Eosin staining was performed following standard protocols. For X-gal staining, embryos were dissected into ice-cold PBS, fresh frozen in optimal cutting temperature (OCT) compound and sectioned at 14 μm. X-gal-stained sections were counterstained with Eosin. For β-gal immunohistochemistry on paraffin sections, a polyclonal rabbit antiserum was raised against full-length denatured and SDS-PAGE-purified *Escherichia coli* β-gal. For β-gal immunohistochemistry on whole-mount cochleas, rabbit anti-β-gal was purchased from 5-prime/3-prime (Boulder, CO, USA). Rabbit anti-OE, anti-adenylyl cyclase type 3, and anti-olfactory marker protein were used as described previously (Bakalyar and Reed, 1990; Wang et al., 1997). Cell proliferation was analyzed by in vivo labeling with ethynyl deoxyuridine (EdU) and Click-iT detection (Salic and Mitchison, 2008) (Invitrogen). EdU (25 mg/kg body weight) was injected intraperitoneally into pregnant mice. Embryos were recovered 2 hours later and fixed, dehydrated and embedded in paraffin. Quantification was performed by counting EdU-positive nuclei per unit area. Apoptosis was assessed on cryosections stained with rabbit anti-cleaved caspase 3 (Cell Signaling).

Electro-olfactogram (EOG) recordings

EOG recordings were performed as described previously (Zhao and Reed, 2001) using 4- and 8-week-old *Fz2*$^{-/-}$ and *Fz2*$^{+/-}$ littermates. Odorants (acetophenone, amyl acetate and heptanal) were from Sigma-Aldrich. Stock solutions of odorants (0.5 M in DMSO) were diluted in water. During the recording session, 2 ml of odorant solution was placed in a sealed 10 ml glass test tube, the air above the solution was allowed to equilibrate with the odorant, and then the gas phase odorant was delivered as a 60 millisecond pulse injected into a continuous stream of humidified air flowing over the tissue sample. EOG electrodes were placed on turbinates IIb or III for continuous recording. Data were analyzed with Clampfit software (Axon Instruments) and the peak heights measured with reference to the pre-pulse baseline. Multiple mutant and wild-type mice were analyzed in each recording session, with the testing sequence alternating between the two types.

Scanning electron microscopy

E13 or E14 palates were fixed overnight in 2.5% glutaraldehyde in 0.1 M sodium cacodylate, osmicated, stained with uranyl acetate, dehydrated, subjected to critical point drying, and coated with 20 nm gold-palladium. Samples were viewed with a Leo 1530 field emission scanning electron microscope.

Skeleton preparation

Skeletons were prepared as described previously (Hogan et al., 1994). In brief, embryos or newborn pups were skinned, eviscerated, and fixed in 95% ethanol overnight. They were then stained in Alcian Blue overnight, washed with ethanol for 2-5 hours, treated with 1% KOH for 24 hours, stained overnight in 1% KOH /0.015% Alizarin Red S, cleared in 1% KOH/20% glycerol for at least 2 days, and stored in glycerol:ethanol (1:1).

Microarray hybridization

Palates were dissected from E13 *Fz1*$^{-/-}$;*Fz2*$^{+/+}$ and *Fz1*$^{-/-}$;*Fz2*$^{-/-}$ embryos. Three to five pairs of palates were pooled for each RNA purification. RNA was extracted using Trizol (Invitrogen) and RNeasy (Qiagen) kits. Three biologically independent pairs of hybridizations were performed with mouse genome 430 2.0 microarrays (Affymetrix). Data were processed as described previously (Chen et al., 2005). Data have been submitted to Gene Expression Omnibus (accession number GSE24276).

Luciferase assays

293/Super TOP Flash (STF) cells (Xu et al., 2004) were seeded into 24-well plates and transfected using Fugene-6 (Roche) with 50 ng of Wnt plasmid, 50 ng of Fz plasmid, 50 ng of Lrp5 plasmid and 0.8 ng of the transfection control Renilla luciferase plasmid pTK-RL (Promega). The DNA mixture was adjusted to 200 ng total per well with the pRK5 vector. Two days after transfection, luciferase activities were measured with a Dual-Luciferase Assay Kit (Promega). The fold induction was derived by dividing normalized reporter activity [firefly luciferase:renilla luciferase ratio (RLU)] for the experimental samples by RLU for the control wells transfected with pRK5 vector alone. Transfections and luciferase assays were performed in triplicate.

Whole-mount cochlea preparations and hair cell analysis

Inner ear dissection was performed as described previously (Wang et al., 2006). Briefly, cochleas from E18 embryos were fixed in 4% PFA in PBS at room temperature for 1 hour, and the organ of Corti was dissected and stained with Texas Red-X phalloidin (Invitrogen). The tissues were visualized using a Zeiss LSM510. For quantification of hair cell numbers, territories encompassing 100 inner hair cells (IHCs) and ~330 outer hair cells (OHCs) at the base, middle and apex of each cochlea were delimited, and the number of missing or excess IHCs and OHCs was counted for each territory. Hair bundle orientations were measured relative to the local alignment of hair cell bodies in confocal images from the base, middle and apex of each cochlea.

Semi-quantitative reverse transcription PCR (RT-PCR)

RNA from three wild-type E13 palates was used as a template for cDNA synthesis followed by PCR with Wnt-specific primers (see Table S2 in the supplementary material).

Statistical analysis

Student's *t*-test and Fisher's two-tailed exact test were used for statistical comparisons (Microsoft Excel and http://graphpad.com/quickcalcs/contingency1.cfm).

RESULTS

Targeted mutation and expression of *Fz1* and *Fz2* genes

An analysis of sequence similarity among the ten mammalian Fz proteins showed that Fz1, Fz2 and Fz7 form a distinct branch within the Fz family (see Fig. S1 in the supplementary material),

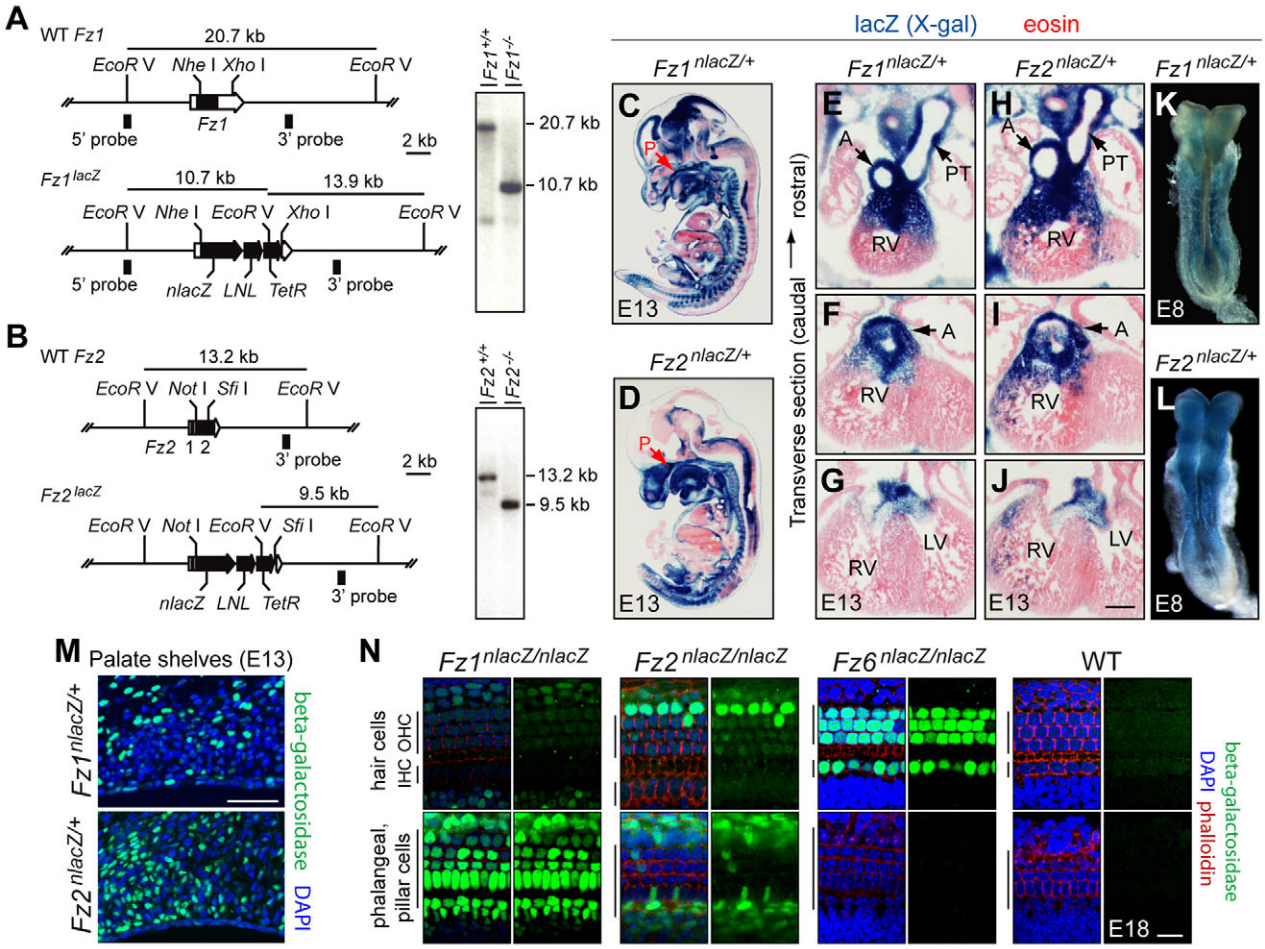

Fig. 1. Targeted mutation of *Fz1* and *Fz2* in mouse and expression of $Fz1^{nlacZ}$ and $Fz2^{nlacZ}$. (**A**,**B**) *Fz1* and *Fz2* knockout/*nlacZ* knock-in strategy. Wild-type (WT) *Fz1* and *Fz2* genes (upper maps), gene knockout/*nlacZ* knock-in alleles (lower maps), and genomic Southern blots (right). Southern blot probes and fragment sizes for *Eco*RV digests are shown. *LNL*, *PGK-neo* cassette flanked by *loxP* sites, later excised by germline Cre-mediated recombination. *TetR*, tetracycline resistance gene. (**C-J**) X-gal staining (blue) at E13 shows distinctive patterns of $Fz1^{nlacZ}$ and $Fz2^{nlacZ}$ expression, including in the developing palate epithelium and mesenchyme (C,D), and at the base of the cardiac outflow tract and the developing aorta and pulmonary trunk (E-J). P, palate; A, aorta; PT, pulmonary trunk; LV, left ventricle; RV, right ventricle. (**K**,**L**) X-gal staining (blue) of $Fz1^{nlacZ/+}$ and $Fz2^{nlacZ/+}$ E8 embryos shows *Fz1* expression principally in the somites and surrounding mesenchyme, and widespread *Fz2* expression, including in the lips of the open neural tube. (**M**) Anti-β-gal immunostaining (green) reveals $Fz1^{nlacZ}$ and $Fz2^{nlacZ}$ expression on the medial walls of the palate shelves at E13. Counterstained with DAPI (blue). (**N**) Anti-β-gal immunostaining (green) reveals $Fz1^{nlacZ}$, $Fz2^{nlacZ}$ and $Fz6^{nlacZ}$ expression in the organ of Corti at E18; a wild-type control is shown on the right. Counterstained with DAPI (blue) and phalloidin (red) in each left-hand panel. The upper and lower rows of images show optical sections at the level of the hair cell nuclei and the underlying phalangeal and pillar cell nuclei, respectively. IHC, inner hair cells; OHC, outer hair cells. Scale bars: in J, 250 μm for E-J; 100 μm in M; 20 μm in N.

suggesting that this subfamily might function in related and/or overlapping processes. To investigate this possibility, we constructed targeted knockouts of *Fz1* and *Fz2* using a nuclear-localized *lacZ* coding region to replace the Fz coding region, which in both genes resides within a single exon (Fig. 1A,B). X-gal staining of $Fz1^{nlacZ/+}$ and $Fz2^{nlacZ/+}$ embryos and adults showed that both genes are expressed in a wide variety of tissues, consistent with previous in situ hybridization, RNA blot and RNAse protection analyses (Fig. 1C-L; see Fig. S2 and Table S1 in the supplementary material) (Chan et al., 1992; van Gijn et al., 2001; Wang et al., 1996). Of particular relevance to the present study, both genes are expressed in the developing palate, cardiac outflow tract and neural tube. In the CNS at E13, *Fz1* was expressed at higher levels in the brain than in the spinal cord, whereas *Fz2* showed the reciprocal pattern (Fig. 1C,D). At E8, just prior to neural tube closure, X-gal staining of $Fz2^{nlacZ/+}$ embryos showed widespread expression, including expression along the entire length of the neural tube (Fig. 1K,L).

Higher resolution analysis using anti-β-gal antibodies showed expression in the palate shelves at E13, ~1 day prior to palate closure, with *Fz1* expression in both the surface epithelium and the underlying mesoderm, and *Fz2* expression confined largely to the mesoderm (Fig. 1M). In the organ of Corti at E18, *Fz1* was expressed weakly in the three outer rows of sensory hair cells and strongly in the flanking non-sensory epithelial cells and the underlying phalangeal and pillar cells (Fig. 1N). *Fz2* also showed stronger expression in supporting cells compared with sensory cells, with the strongest expression in a single row of non-sensory epithelial cells immediately beyond the third row of outer hair cells (Fig. 1N). *Fz6* expression (analyzed with an analogous *nlacZ*

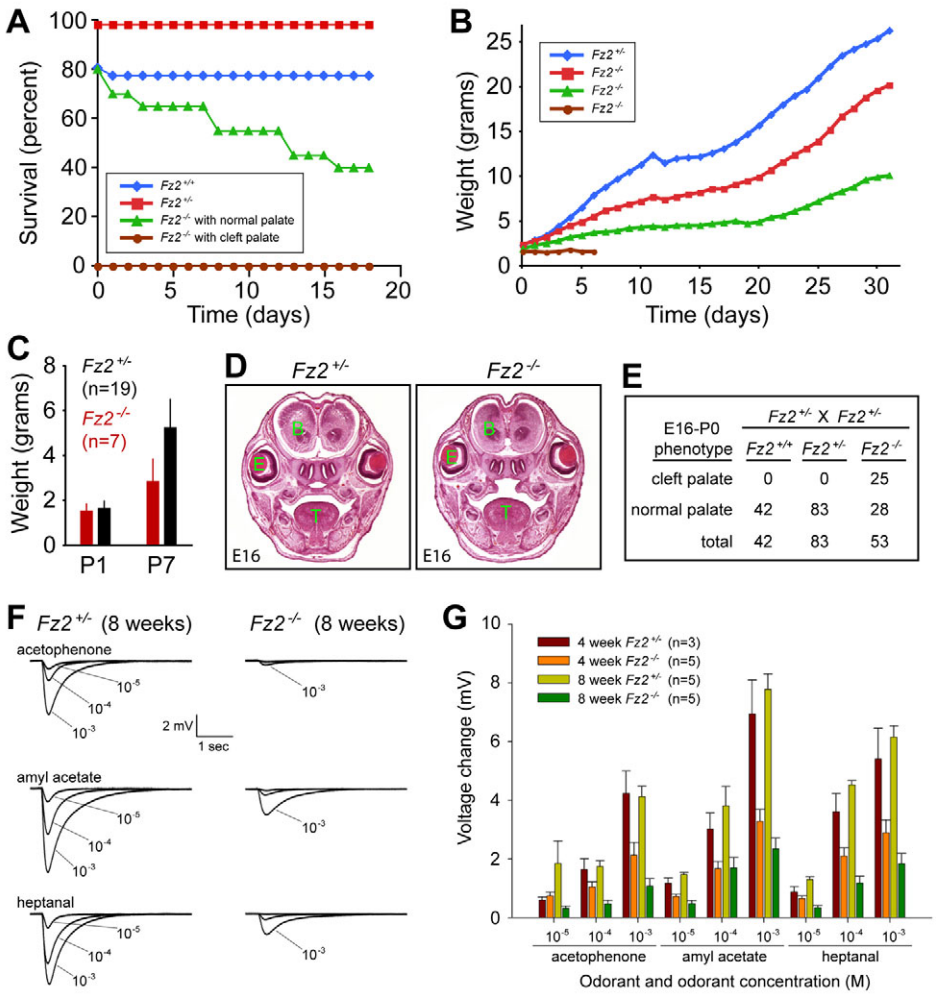

Fig. 2. Failure to thrive, cleft palate and olfactory defects in *Fz2*$^{-/-}$ mice. (**A**) Postnatal survival curves for *Fz2*$^{+/+}$ (*n*=31), *Fz2*$^{+/-}$(*n*=54), and *Fz2*$^{-/-}$ (*n*=20 with normal palate; *n*=19 with cleft palate). In this cohort, 20% of *Fz2*$^{+/+}$ and 20% of *Fz2*$^{-/-}$ neonates died, values that are within the range of normal variation for wild-type mice. (**B**) Variable manifestation of the failure-to-thrive phenotype among postnatal *Fz2*$^{-/-}$ mice with closed palates; daily postnatal weights are shown for one representative *Fz2*$^{+/-}$ mouse and three *Fz2*$^{-/-}$ littermates, one of which died at P6. (**C**) Mean weight ± s.d. at P1 and P7 for *Fz2*$^{+/-}$(*n*=19) and *Fz2*$^{-/-}$ (*n*=7) mice. At P7 *P*=0.0015 (Student's *t*-test). (**D**) Coronal sections at E16 showing the cleft palate in *Fz2*$^{-/-}$ embryos. B, brain; E, eye; T, tongue. (**E**) *Fz2*$^{-/-}$ mice were found at the expected Mendelian frequency at late gestation and at birth; ~50% have cleft palate. *P*-value for cleft palate for *Fz2*$^{-/-}$ versus *Fz2*$^{+/-}$ and *Fz2*$^{+/+}$=1.3×10^{-15} (χ^2 test). (**F**) Electro-olfactogram (EOG) responses in *Fz2*$^{+/-}$ and *Fz2*$^{-/-}$ littermates at 8 weeks of age. Three odorants were applied as single puffs of vapor from an aqueous solution at the indicated odorant concentration (in moles/liter). (**G**) Mean EOG amplitude ± s.d. among littermates at 4 and 8 weeks of age.

knock-in) (Wang et al., 2006) was largely confined to sensory hair cells (Fig. 1N). In all of the anti-β-gal analyses, the *nlacZ* reporter showed variegated expression.

Failure to thrive and palate clefting in *Fz2*$^{-/-}$ mice

Fz1$^{-/-}$ mice were healthy and fertile and exhibited no orofacial or cardiac anomalies. By contrast, ~50% of *Fz2*$^{-/-}$ mice had a cleft palate and died as neonates, and the ~50% that survived exhibited a variable degree of runting that developed during the early postnatal period (Fig. 2A-D). The penetrance of these two phenotypes was equivalent on a mixed C57Bl/6 × Sv129 background and a pure Sv129 background. Intra-uterine survival did not require *Fz2*, as *Fz2*$^{-/-}$ fetuses and neonates, including those with cleft palates, were found at the expected Mendelian frequency (Fig. 2E). At present, the mechanistic basis of the failure-to-thrive phenotype among postnatal *Fz2*$^{-/-}$ mice remains obscure. Blood cell counts, levels of serum electrolytes, and urine protein and glucose were within the normal ranges, and anterior pituitary histology (including growth hormone and adrenocorticotropic hormone immunohistochemistry), gastrointestinal histology, complete serial histological and magnetic resonance imaging (MRI) analyses of the brain, and skeleton preparations all closely matched those of wild-type (WT) littermates (but with reduced size of the anatomical structures; data not shown). As impaired feeding and failure-to-thrive phenotypes have previously been reported in mice with a primary defect in olfaction (Belluscio et al., 1998; Zhao and Reed, 2001), we analyzed the function of the olfactory epithelium in 4- and 8-week-old littermates by EOG, which reveals the summed electrical response of the olfactory epithelium to various odorants (Fig. 2F,G). This analysis demonstrated substantially reduced EOG responses in *Fz2*$^{-/-}$ mice. Although the EOG data indicated that *Fz2*$^{-/-}$ mice have reduced olfactory sensitivity, the olfactory bulbs of *Fz2*$^{-/-}$ mice appeared to be morphologically normal, and immunohistochemical analyses of the olfactory epithelium using the neuronal markers olfactory marker protein (Omp), adenylyl cyclase type 3 (AC3; Adcy3 – Mouse Genome Informatics), and olfactory epithelium/EBF (OE) transcription factors showed little or no difference between *Fz2*$^{-/-}$ and *Fz2*$^{+/-}$ (see Fig. S3 in the supplementary material). As our attempts to increase weight gain in *Fz2*$^{-/-}$ pups by supplementary feeding with infant formula or by removing competing WT siblings met with minimal success, the contribution of the olfactory defect to the failure-to-thrive phenotype is likely to be modest.

Fully penetrant palate clefting in *Fz1*$^{-/-}$;*Fz2*$^{-/-}$ mice

The overlapping patterns of *Fz1* and *Fz2* expression in the developing palate (Fig. 1C,D,M; see Fig. S2 in the supplementary material) suggested the potential for partial redundancy during palate closure, a process that is sensitive to a variety of genetic perturbations (Jugessur and Murray, 2005). Consistent with this

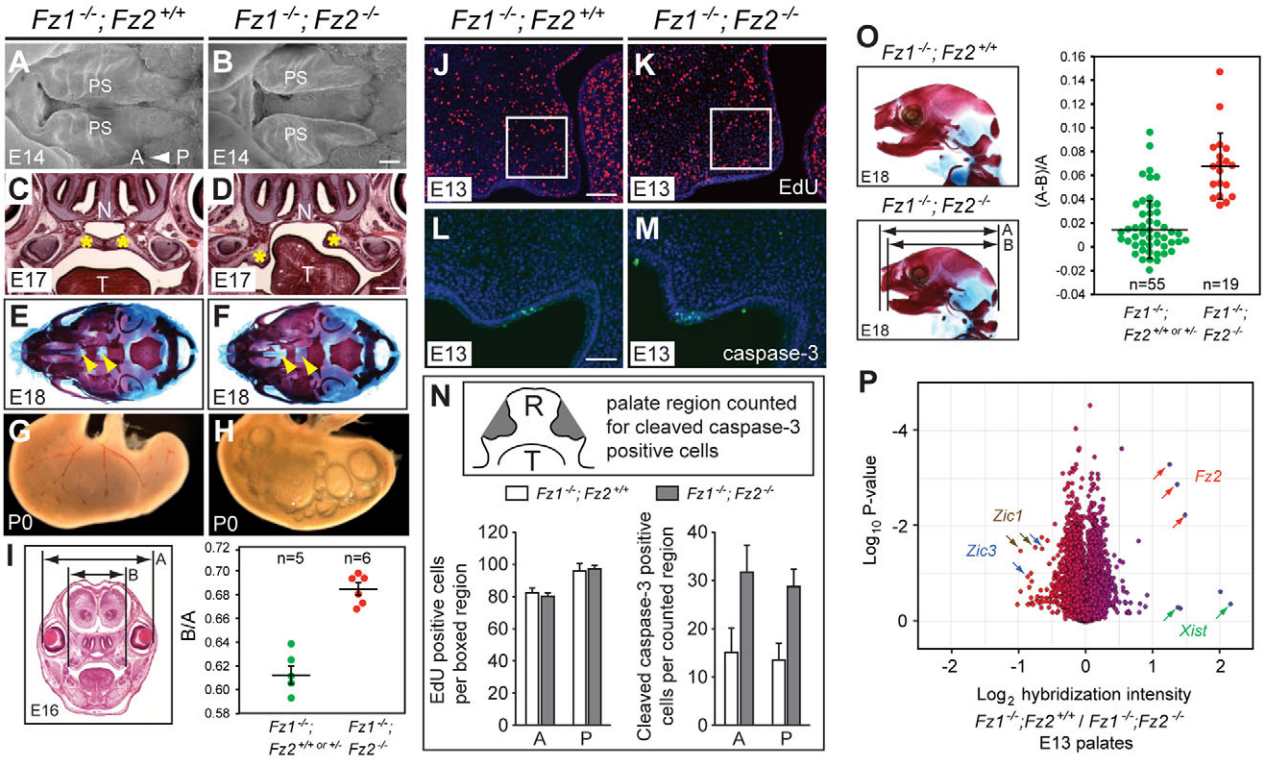

Fig. 3. Craniofacial defects in *Fz1*$^{-/-}$;*Fz2*$^{-/-}$ mice. (**A**,**B**) Scanning electron microscopy of the developing palate at E14 (ventral view). The palate shelves (PS) are partially closed in phenotypically wild-type *Fz1*$^{-/-}$;*Fz2*$^{+/+}$ embryos (A), but they show minimal movement towards the midline in a *Fz1*$^{-/-}$;*Fz2*$^{-/-}$ littermate (B). A, anterior; P, posterior. (**C**,**D**) Coronal sections at E17. Yellow asterisks indicate palate shelves. N, nares; T, tongue. In the *Fz1*$^{-/-}$;*Fz2*$^{-/-}$ embryo, failure of palate shelf elevation on the left side can be seen. (**E**,**F**) Ventral views of the skull at E18; palatine bones (yellow arrowheads) are missing in the *Fz1*$^{-/-}$;*Fz2*$^{-/-}$ skull. (**G**,**H**) Characteristic accumulation of air bubbles in the stomach of an *Fz1*$^{-/-}$;*Fz2*$^{-/-}$ mouse at P0. (**I**) Widening of the roof of the mouth in *Fz1*$^{-/-}$;*Fz2*$^{-/-}$ mice with open palates compared with *Fz1*$^{-/-}$;*Fz2*$^{+/+}$ and *Fz1*$^{-/-}$;*Fz2*$^{+/-}$ littermates with closed palates at E16. The relative distances between the upper molars (marked B) and the outer edges of the lenses (marked A) are plotted as the ratio B/A. $P=1.4\times10^{-4}$ (Student's *t*-test). (**J-M**) EdU incorporation (J,K; left palate shelf) and anti-cleaved caspase 3 (L,M; right palate shelf) in coronal sections through the anterior region of E13 *Fz1*$^{-/-}$;*Fz2*$^{+/+}$ and *Fz1*$^{-/-}$;*Fz2*$^{-/-}$ palates. Boxes (J,K) indicate the area in which EdU-labeled cells were counted. (**N**) Mean ± s.d. of EdU (n=4 mice) and anti-cleaved caspase-3 (n=3 mice) labeled cells, from anterior (A) and posterior (P) regions of the palate. Inset is a schematic of a coronal section showing the palate shelf regions (gray) analyzed for anti-cleaved caspase-3-labeled cells. R, roof of the mouth; T, tongue. (**O**) Hypognathia in *Fz1*$^{-/-}$;*Fz2*$^{-/-}$ mice at E18, compared with phenotypically wild-type *Fz1*$^{-/-}$;*Fz2*$^{+/+}$ littermates. Mean ± s.d. relative distances from the back of the skull to the anterior tip of the upper jaw (marked A) or lower jaw (marked B) [calculated as (A-B)/A]. P-value=2.2×10^{-7} (Student's *t*-test). (**P**) Microarray hybridization of RNA from E13 *Fz1*$^{-/-}$;*Fz2*$^{+/+}$ (wild type) versus *Fz1*$^{-/-}$;*Fz2*$^{-/-}$ palates show minimal differences in three independent biological replicates with three to five bilateral palates pooled per sample. The scatter plot shows the $\log_2$ of the average of *Fz1*$^{-/-}$;*Fz2*$^{+/+}$ divided by *Fz1*$^{-/-}$;*Fz2*$^{-/-}$ transcript abundances on the *x*-axis and the $\log_{10}$ P-value on the *y*-axis. Arrows indicate transcripts: red, *Fz2*; green, *Xist*; brown, *Zic1*; blue, *Zic3*. Scale bars: 200 μm in B; 500 μm in D; 100 μm in J; 50 μm in L.

idea, late gestation *Fz1*$^{-/-}$;*Fz2*$^{-/-}$ fetuses exhibited palate clefting with greater than 99% penetrance (n=180 mice). *Fz1*$^{-/-}$;*Fz2*$^{-/-}$ neonates typically appeared cyanotic and accumulated air in their stomachs, presumably owing to the connection between oral and nasal cavities (Fig. 3A-H). The near absence of cleft palate in *Fz1*$^{-/-}$;*Fz2*$^{+/-}$ embryos (n=2/208) suggests that *Fz2* gene dosage is more important than *Fz1* dosage, consistent with the higher expression level of *Fz2* relative to *Fz1* in the palate (Fig. 1C,D,M; see Fig. S2 in the supplementary material).

In *Fz1*$^{-/-}$;*Fz2*$^{-/-}$ embryos, the palate shelves invariably failed to meet at the midline; in many cases they also failed to elevate, as seen for the left palate shelf in Fig. 3D. Quantification of the width of the roof of the mouth at E16, as determined by measuring the distance between the upper molars and normalizing this distance to the inter-ocular distance, showed that *Fz1*$^{-/-}$;*Fz2*$^{-/-}$ embryos have a wider roof relative to controls, an observation that suggests the failure of a convergent-extension process (Fig. 3I). The failure of palate shelf elevation and midline extension does not appear to have arisen from differential rates of cell proliferation during palatogenesis, as the levels of EdU incorporation in the palate at E13 and E14 were indistinguishable among *Fz1*$^{-/-}$;*Fz2*$^{-/-}$ and *Fz1*$^{-/-}$;*Fz2*$^{+/+}$ littermates (Fig. 3J-N). This morphogenetic failure could potentially be related to the observed ~2-fold increase in the number of apoptotic cells in *Fz1*$^{-/-}$;*Fz2*$^{-/-}$ compared with *Fz1*$^{-/-}$;*Fz2*$^{+/+}$ palates at E13 (Fig. 3L-N), most of which were located in the epithelial layer. However, the number of apoptotic cells was extremely small in both control and defective palates; therefore, we suspect that their excess in the *Fz1*$^{-/-}$;*Fz2*$^{-/-}$ palate is more likely to represent a secondary consequence of the underlying failure of palate shelf movement, rather than its primary cause. In addition to an open palate, late gestational and neonatal *Fz1*$^{-/-}$;*Fz2*$^{-/-}$ mice exhibited shortened lower jaws (hypognathia; Fig. 3O). No other skeletal anomalies were observed among the 19 *Fz1*$^{-/-}$;*Fz2*$^{-/-}$ mice examined.

A Cardiovascular defects detected in Fz1 Fz2 embryos (E16 - E18)

Cardiovascular defects	*Fz1*$^{-/-}$	*Fz2*$^{-/-}$	*Fz1*$^{-/-}$;*Fz2*$^{+/-}$	*Fz1*$^{+/-}$;*Fz2*$^{-/-}$	*Fz1*$^{-/-}$;*Fz2*$^{-/-}$
Ventricular septal defect (VSD)	0/11	0/11	0/8	1/6	7/22
Double outlet right ventricle (DORV)	0/11	0/11	0/8	0/6	1/22
Over-riding aorta	0/11	0/11	1/8	0/6	0/22
VSD + DORV	0/11	0/11	0/8	0/6	7/22
VSD + Over-riding aorta	0/11	0/11	0/8	0/6	1/22
Total	0/11	0/11	1/8	1/6	16/22

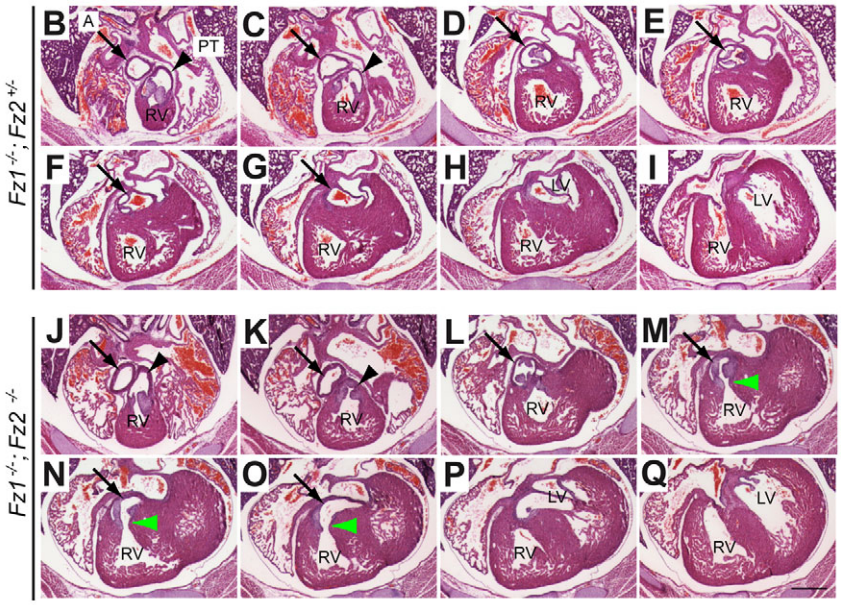

Fig. 4. Cardiac defects in *Fz1*$^{-/-}$;*Fz2*$^{-/-}$ embryos. (**A**) Summary of late gestational cardiac phenotypes among progeny with various combinations of *Fz1* and/or *Fz2* mutations. Serial transverse sections were analyzed from 58 late gestational fetuses. (**B-Q**) Rostral-to-caudal transverse sections from a phenotypically wild-type E16 *Fz1*$^{-/-}$;*Fz2*$^{+/-}$ embryo (B-I) and an E16 *Fz1*$^{-/-}$;*Fz2*$^{-/-}$ embryo with ventricular septal defects (VSD) and double outlet right ventricle (DORV) (J-Q). Green arrowheads in M-O indicate the abnormal connection between the aorta and the right ventricle. A, aorta (black arrow); PT, pulmonary trunk (black arrowhead); LV, left ventricle; RV, right ventricle. Scale bar: 500 μm.

The function of Fz1 and Fz2 in palate closure can be simplistically conceptualized in two mutually exclusive models: (1) regulation of the transcriptome (canonical Wnt signaling), or (2) regulation of cytoskeletal or other cytosolic processes in a manner that is largely or completely independent of changes in the transcriptome (non-canonical Wnt signaling). To make a rough distinction between these models, we microdissected E13 palates from *Fz1*$^{-/-}$;*Fz2*$^{+/+}$ and *Fz1*$^{-/-}$;*Fz2*$^{-/-}$ embryos and compared transcript abundances by hybridization to Affymetrix 430 2.0 gene chips (Fig. 3P). The result of a comparison across three biologically independent experiments was remarkable because of the near identity in transcript abundances between the two genotypes: only a few transcripts exhibited greater than 2-fold changes. Among these, one codes for Fz2 (as expected) and a second is Xist, reflecting random variation in gender among embryos. With the possible exception of *Zic1* and *Zic3* transcripts, which are more abundant in *Fz1*$^{-/-}$;*Fz2*$^{-/-}$ compared with control palates, the small number of transcripts with abundance changes between 1.5- and 2-fold were generally not statistically significant. The *Zic* gene family has been implicated in the control of cell proliferation and neural development, including neural tube closure, in mice and humans (Grinberg and Millen, 2005; Inoue et al., 2007). Similar results were also obtained with E14 palates (data not shown). Although we cannot rule out the possibility that Fz1 and Fz2 critically affect transcript abundances in only a small proportion of palate cells, the microarray data suggest that Fz1 and Fz2 might act in this context through post-transcriptional mechanisms.

Several Wnts have been implicated in palate closure: palate clefting is observed with full penetrance in *Wnt5a*$^{-/-}$ mice (He et al., 2008) and with partial penetrance in *Wnt9b*$^{-/-}$ mice (Juriloff et al., 2006); *WNT3* mutations have been identified in a human syndrome that includes cleft palate (Niemann et al., 2004), and mouse palate explant experiments suggest that Wnt11 functions in the terminal fusion process (Lee et al., 2008). To examine potential Wnt/frizzled interactions in the palate, we used RT-PCR to survey E13 palates for the presence of transcripts coding for each of the 19 mammalian Wnt proteins (see Fig. S4 and Table S2 in the supplementary material). This survey revealed a remarkably complex picture, with expression of at least 11 Wnt genes detected at the time of palate shelf elevation and closure. Similar results have recently been reported by Warner et al. (Warner et al., 2009). Curiously, three of the four Wnts noted above (*Wnt3*, *Wnt9b* and *Wnt11*) were below the limits of detection of our RT-PCR assay. To test whether Wnt3, 5a, 9b, or 11 could be relevant to canonical Wnt signaling via Fz1 and/or Fz2, we co-transfected various combinations of cDNAs coding for these Wnt and Fz proteins, together with the co-receptor Lrp5, into a luciferase reporter cell line for canonical Wnt signaling (STF cells) (Xu et al., 2004) (see Fig. S5 in the supplementary material). Relative to a positive control in which co-transfection of Wnt9b, Fz5 and Lrp5 produces a signal at least 100-fold over background, we observed little or no canonical signaling by Fz1 or Fz2 in combination with Wnt5a or Wnt11, but robust activation of canonical signaling by Fz1 and Fz2 in combination with Wnt3 or Wnt9b. These data suggest the possibility that Wnt3 and Wnt9b (and perhaps other Wnts) might act during palatogenesis by canonical Wnt signaling via Fz1 and Fz2.

High frequency of cardiac defects in *Fz1*$^{-/-}$;*Fz2*$^{-/-}$ embryos

Thus far, no frizzled genes have been implicated in cardiac development. The plausibility of a role for *Fz1* and *Fz2* in cardiac development was suggested by their expression in the developing outflow tract and adjacent cardiac tissue (Fig. 1E-J) (van Gijn et

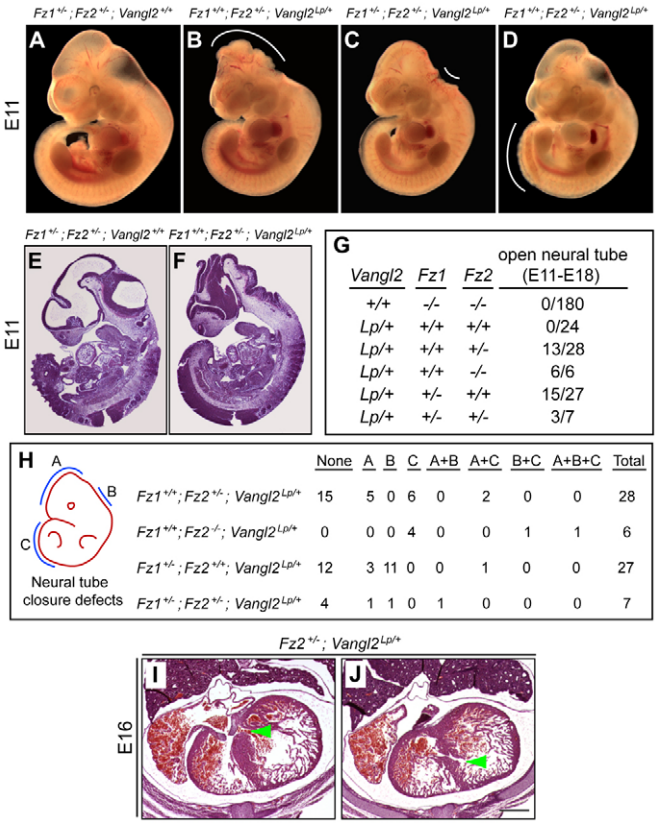

Fig. 5. Genetic interactions between *Fz1*, *Fz2* and *Vangl2* in neural tube closure and heart development. (**A-G**) A variety of neural tube defects (NTDs; white arcs) were observed when different combinations of *Fz1* and/or *Fz2* alleles were combined with *Vangl2*$^{Lp/+}$; NTDs were not observed among *Vangl2*$^{+/+}$ littermates carrying the same combinations of *Fz1* and *Fz2* alleles. Sagittal sections at E11 show normal cephalic neural tube closure in a *Fz1*$^{+/-}$;*Fz2*$^{+/-}$;*Vangl2*$^{+/+}$ embryo (E) and the failure of cephalic neural tube closure in a *Fz1*$^{+/+}$;*Fz2*$^{+/-}$;*Vangl2*$^{Lp/+}$ embryo (F). (**H**) Locations of NTDs along the neuraxis among double- and triple- mutant embryos. Zones A, B and C represent the cephalic, cervical and caudal regions, respectively, as shown in the schematic on the left. (**I**,**J**) Transverse sections through an E16 *Fz2*$^{+/-}$;*Vangl2*$^{Lp/+}$ heart show both membranous ventricular septal defects (VSD; green arrowhead in I) and muscular VSD (green arrowhead in J). Scale bar: in J, 500 µm for I,J.

al., 2001). To test whether *Fz1* and/or *Fz2* play a role in this process, the heart and great vessels were examined by serial sectioning of embryos from E16 to E18 (Fig. 4). Among 22 *Fz1*$^{-/-}$;*Fz2*$^{-/-}$ embryos, 16 had either a ventricular septal defect (VSD), an overriding aorta, double outlet right ventricle (DORV) or some combination of VSD and one of the other two anomalies. By contrast, only one out of eight *Fz1*$^{-/-}$;*Fz2*$^{+/-}$ and one out of six *Fz1*$^{+/-}$;*Fz2*$^{-/-}$ embryos had a cardiac defect, and none of the *Fz1*$^{-/-}$ or *Fz2*$^{-/-}$ embryos had cardiac anomalies. These data reveal a redundant role for *Fz1* and *Fz2* in cardiac outflow tract development and in closure of the ventricular septum. The incomplete penetrance of the cardiac phenotype in *Fz1*$^{-/-}$;*Fz2*$^{-/-}$ embryos suggests that additional frizzled proteins might be involved. At present, the mechanism by which the cardiac defect occurs is unclear. A failure of cardiac neural crest migration secondary to a general defect in neural crest migration seems to be unlikely because the dorsal root ganglia and thymic rudiments – both of which require neural crest migration – are unaffected in *Fz1*$^{-/-}$;*Fz2*$^{-/-}$, *Fz1*$^{-/-}$;*Fz2*$^{+/-}$ and *Fz1*$^{-/-}$;*Fz2*$^{+/+}$ embryos.

Genetic interactions between *Fz1*, *Fz2* and *Vangl2* mutations

The experiments described above establish essential roles for Fz1 and Fz2 in palate closure and cardiac development, but they do not provide any link between these proteins and other cell signaling components. Of relevance to the possibility of such a link, we noted that: (1) the minimal change in transcript abundances in *Fz1*$^{-/-}$;*Fz2*$^{-/-}$ versus control palates (Fig. 3P) suggests that the functions of Fz1 and Fz2 in this context might involve PCP rather than canonical Wnt signaling, as the latter involves changes in gene transcription; (2) palate closure requires Wnt5a, and cardiac outflow tract development requires Wnt5a, Wnt11 and Vangl2 (Henderson et al., 2006; He et al., 2008; Cohen et al., 2008; Zhou et al., 2007), all of which are connected to non-canonical or PCP signaling; and (3) there is a rough anatomical similarity between closure of the palate, ventricular septum, neural tube and eyelid, suggesting that all four processes might utilize some of the same molecular mechanisms. These considerations led us to test whether *Fz1* and *Fz2* might genetically interact with *Vangl2*, a core PCP component.

For these experiments, we used the *Vangl2 loop-tail* (*Lp*) allele. *Vangl2*$^{Lp/+}$ mice have a curled tail and reduced female fertility, whereas *Vangl2*$^{Lp/Lp}$ mice die at birth with a fully open neural tube, open eyelids, and disorganized and misorientated inner ear sensory hair cells; *Vangl2*$^{Lp/Lp}$ mice do not have a defect in palate closure (Kibar et al., 2001; Montcouquiol et al., 2003; Murdoch et al., 2001). In crosses that generated various compound heterozygote combinations for *Vangl2*, *Fz1* and/or *Fz2*, we observed a high frequency of neural tube defects (NTDs) among *Fz1*$^{+/-}$;*Vangl2*$^{Lp/+}$, *Fz2*$^{+/-}$;*Vangl2*$^{Lp/+}$ and *Fz1*$^{+/-}$;*Fz2*$^{+/-}$;*Vangl2*$^{Lp/+}$ embryos and in six out of six *Fz2*$^{-/-}$;*Vangl2*$^{Lp/+}$ embryos (Fig. 5A-H; see Table S3 in the supplementary material). Control *Vangl2*$^{Lp/+}$ mice did not exhibit NTDs (n=24); neither did *Fz1*$^{-/-}$;*Fz2*$^{-/-}$ embryos (n=180) nor various *Fz1* and *Fz2* combinations with three or fewer Fz null alleles (e.g. *Fz1*$^{-/-}$;*Fz2*$^{+/-}$; n=208). Interestingly, the NTDs seen in compound heterozygotes between *Vangl2* and *Fz1* and/or *Fz2* were distributed at a variety of locations along the neuraxis: NTDs associated with heterozygosity for *Fz1* were more common in the rostral neural tube, whereas NTDs associated with homozygous deletion of *Fz2* were more common in the caudal neural tube (Fig. 5H). Additionally, we examined the heart in six of the E16-18 embryos with NTDs and observed two with muscular VSD and one with both membranous and muscular VSDs (Fig. 5I,J). The *Vangl2*$^{Lp/+}$ background had no effect on the incidence of cleft palate when combined with *Fz2*$^{-/-}$ (two out of six had a cleft palate compared with the expected 50%; Fig. 2D), and no palate clefting was observed among 54 late gestation embryos with *Vangl2*$^{Lp/+}$ in combination with *Fz1*$^{+/-}$ and/or *Fz2*$^{+/-}$.

Additional evidence for an interaction between *Fz2* and *Vangl2* was found in the cochlea, where both *Fz1* and *Fz2* are expressed at low levels in sensory hair cells, and at higher levels in the underlying supporting cells and the surrounding non-sensory epithelium (Fig. 1N). For these experiments, we examined and quantified E18 hair cell numbers (n=35,000 cells) and orientations (n=3000 cells) in *Fz1*$^{+/-}$ (which served as control; n=3 embryos) versus *Fz2*$^{-/-}$ (n=4 embryos) cochleas, and *Vangl2*$^{Lp/+}$ (n=5 embryos) versus *Fz2*$^{-/-}$;*Vangl2*$^{Lp/+}$ (n=4 embryos) cochleas. The phenotype in *Fz2*$^{+/-}$;*Vangl2*$^{Lp/+}$ organs of Corti (n=3 embryos) was,

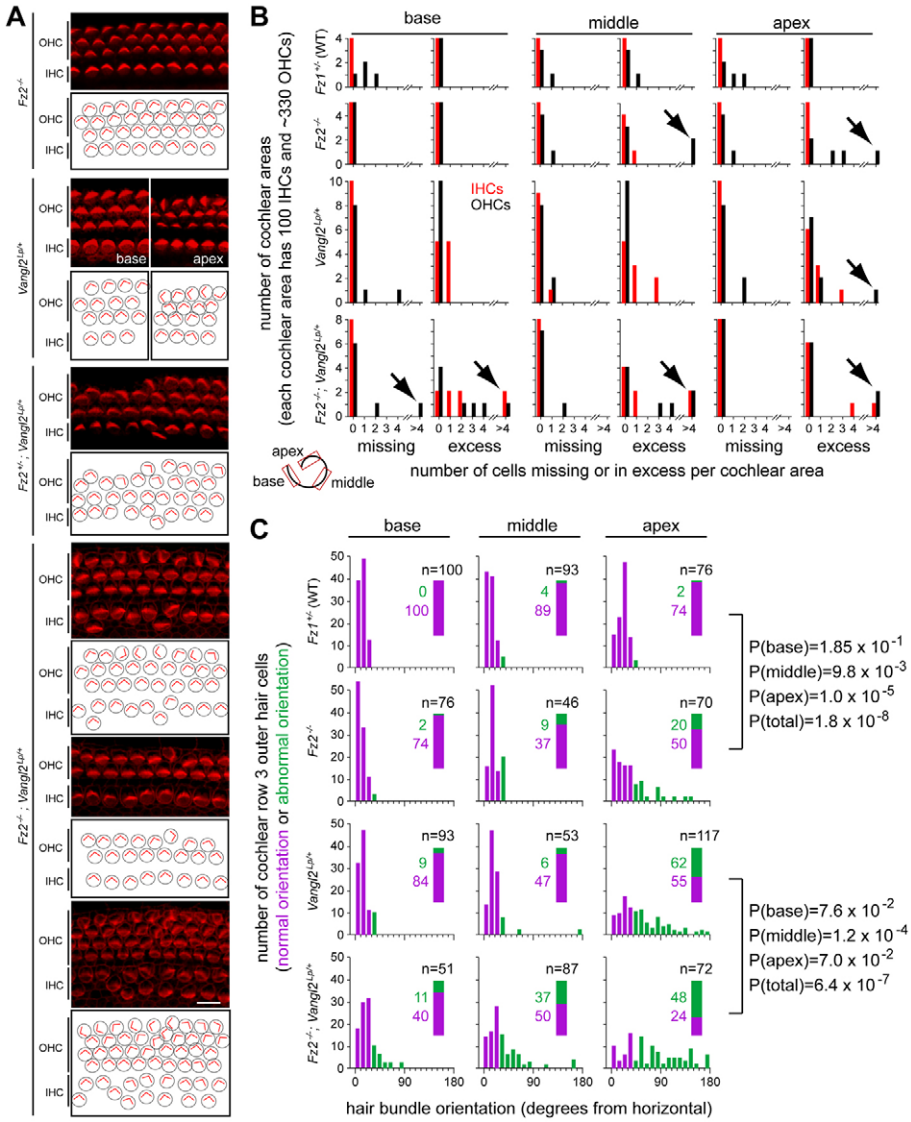

Fig. 6. Genetic interactions between *Fz2* and *Vangl2* in auditory hair cell development. (**A**) Representative phalloidin-stained organ of Corti flat-mounts. The $Fz2^{+/-};Vangl2^{Lp/+}$ tissue is P0; all others are E18. $Fz2^{-/-}$ and $Fz2^{+/-};Vangl2^{Lp/+}$ images are from the middle cochlea. Images from the base and apex are shown for the $Vangl2^{Lp/+}$ sample to illustrate the gradient of hair cell misorientation along the cochlea. The three images of a $Fz2^{-/-};Vangl2^{Lp/+}$ organ of Corti are from the embryo with the most severe phenotype; they show inappropriate numbers, mislocalization and misorientation of hair cells in the middle (upper two panels) and apex (lower panel) of the cochlea. Beneath each image is a schematic showing hair cell locations and hair bundle orientations. IHC, inner hair cells. OHC, outer hair cells. Scale bar in bottom panel: 10 μm. (**B**) Quantification of hair cell number in territories of 100 IHCs and ~330 OHCs sampled from the base, middle and apex of the cochlea at E18, as shown in the schematic in the lower left corner. Red bars, IHCs. Black bars, OHCs. Black arrows highlight deviations of greater than 4 cells. (**C**) Quantification of OHC3 hair bundle orientations. Based on a 95% cut-off in the distribution of hair bundle orientations observed in the $Fz1^{+/-}$ control (upper row), orientations were divided into 'normal' (purple) or 'abnormal' (green) groups. For each region (base, middle or apex) and genotype, the number of hair cells in each category is shown with the green and purple rectangular insets. The corresponding *P*-values (Fisher's two-tailed exact test) for comparisons between genotypes that differ by the presence or absence of *Fz2* are shown to the right.

on average, only modestly more severe than that of $Vangl2^{Lp/+}$ controls (Fig. 6A) and therefore this genotype was not included in the quantitative analysis. For hair cell quantification, we analyzed the base, middle and apex of the cochlea separately because there is a base-to-apex gradient in the maturity of cochlear hair cells.

Fig. 6A shows a series of E18 organ of Corti flat-mounts stained with phalloidin to visualize sensory hair bundle orientations. The normal arrangement of a single row of inner hair cells (IHCs) and three rows of outer hair cells (OHCs) is shown in the $Fz2^{-/-}$ example (Fig. 6A, top panel). The $Vangl2^{Lp/+}$ example illustrates the typical increase in variability in OHC row 3 (OHC3) hair bundle orientation in this mutant background proceeding from base to apex (Fig. 6A, second panel from top). Deviations from the normal number of hair cells – either missing or excess cells – were found in many of the mutant cochleas (Fig. 6A, lower four panels). For quantitative purposes, all deviations of greater than four hair cells per territory were pooled into a single category (Fig. 6B). Of each of the four rows of hair cells, OHC3 was found to exhibit the greatest variation in hair bundle orientation; the comparisons shown in Fig. 6C are therefore restricted to OHC3.

Fig. 6B,C shows that loss of *Fz2*, in either the presence or absence of $Vangl2^{Lp/+}$, produced defects in both hair cell number and OHC3 orientation. For hair cell number, when we dichotomized the sample by taking greater than 4 extra or missing cells per territory as a cut-off for phenotypic deviation, the difference between $Vangl2^{Lp/+}$ and $Fz2^{-/-};Vangl2^{Lp/+}$ was statistically significant (P=0.0014; Fisher's two-tail exact test). For the comparison of $Fz1^{+/-}$ control versus $Fz2^{-/-}$, the sample size was too small to reveal statistical significance (Fig. 6B). For hair bundle orientation, we dichotomized the sample using a cut-off for 'normal' versus 'abnormal' orientations set at the 95th percentile of the $Fz1^{+/-}$ control distribution (top row of Fig. 6C; these categories are shown in purple and green, respectively). Loss of *Fz2*, in either the presence or absence of $Vangl2^{Lp/+}$, disorganized OHC3 orientation with high statistical significance (Fig. 6C).

The $Vangl2^{Lp/+}$ genotype conferred a degree of disorganization in hair cell number and orientation comparable to the loss of *Fz2* (Fig. 6B,C). It is interesting that OHC3 exhibited the highest propensity for hair bundle orientation defects. The observation that *Fz2* expression was high in the row of supporting cells immediately distal to OHC3 (Fig. 1N) suggests that polarity signals from non-

sensory epithelial cells to the adjacent hair cells might be important for orientating hair bundles, as is almost certainly the case in the vestibular system, where each sensory hair cell is completely surrounded by non-sensory epithelial cells, all of which exhibit polarized expression of PCP proteins (Wang et al., 2006; Deans et al., 2007).

Collectively, the results shown in Figs 5 and 6 suggest that *Fz1* and *Fz2* have a PCP-like role in neural tube closure, that *Fz2* has a PCP-like role in inner ear hair cell development and that defects in these functions can be revealed and/or enhanced by perturbing *Vangl2* function.

DISCUSSION

The results presented above show that *Fz1* and *Fz2* are essential for the closure of the palate and of the ventricular septum and for the correct positioning of the cardiac outflow tract. These genes also interact genetically with *Vangl2* to effect neural tube closure, and *Fz2* functions in organizing inner ear sensory hair cells. These results reveal a role for frizzled signaling in a variety of tissue closure processes.

Fz1 and *Fz2* in PCP versus canonical Wnt signaling

A large and diverse set of gene mutations can produce defects in palate closure, ventricular septum closure or positioning of the cardiac outflow tract, implicating a variety of signaling pathways in these processes (Gritli-Linde, 2007; Cohen et al., 2008). Among mice with mutations in PCP-related genes, several exhibit defects in these processes: mutations in *Wnt5a* cause cleft palate (He et al., 2008) and mutations in various Vangl and Dvl family members, either singly or in combination, cause ventricular septal defects and/or cardiac outflow tract anomalies (Etheridge et al., 2008; Henderson et al., 2006; Phillips et al., 2005; Schleiffarth et al., 2007). The partial overlap of phenotypes between $Fz1^{-/-};Fz2^{-/-}$ mice and mice with mutations in other PCP genes, together with the observation of genetic interactions between *Fz1*, *Fz2* and *Vangl2* suggests that Fz1 and Fz2 can act in vivo via PCP signaling in some contexts. It is interesting that in cell culture Fz1 and Fz2 can also mediate canonical Wnt signaling when co-expressed with Wnt3 or Wnt9b (see Fig. S5 in the supplementary material), and that *Lrp6* mutations are also associated with tissue closure defects. Current evidence indicates that the relative strength of canonical and non-canonical Wnt signaling varies in a reciprocal manner and that proteins such as inversin modulate this balance (Simons et al., 2005). It will be interesting to determine whether Fz1 and Fz2 signaling is modulated in this manner in vivo.

When considering whether PCP signaling plays a role in palate closure, two aspects of the $Fz1^{-/-};Fz2^{-/-}$ phenotype seem particularly relevant. First, the microarray data showed very few statistically significant differences when comparing $Fz1^{-/-};Fz2^{-/-}$ with WT palates just prior to, and following, normal palate closure (E13 and E14, respectively). A similar observation has been made when comparing $Fz3^{-/-}$ with WT forebrain transcripts, despite the presence of massive defects in forebrain axon guidance in the $Fz3^{-/-}$ forebrain, and when comparing $Fz6^{-/-}$ with WT skin transcripts in late embryogenesis, despite the nearly random hair follicle orientations in $Fz6^{-/-}$ skin (Y.W. and J.N., unpublished). These results suggest that minimal changes in transcript abundances might be a general feature of PCP signaling. By contrast, in one canonical Wnt signaling system, microarray comparisons of $Fz4^{-/-}$ with WT retinal endothelial cells show numerous statistically significant differences in transcript abundance (Ye et al., 2009). Although we cannot rule out the possibility that a minor cell population exhibits changes in transcript abundance that are below the threshold of detection in our palate microarray experiments, these data suggest that Fz1 and Fz2 could function during palate closure through PCP signaling rather than canonical Wnt signaling. A second aspect of the $Fz1^{-/-};Fz2^{-/-}$ phenotype that suggests a connection between PCP signaling and palate closure is the overall similarity of tissue movements during palate and neural tube closure (Keller, 2002; Tudela et al., 2002). Our observation that $Fz1^{-/-};Fz2^{-/-}$ embryos with open palates have a wider roof of the mouth than WT controls (Fig. 3I), together with similar observations from other mouse models with cleft palate (Gong and Eulenberg, 2001), also support the idea that, in some cases, palate clefting could represent the failure of a convergent-extension-like process.

Tissue closure and common congenital anomalies in humans

One of the central insights to emerge from the study of metazoan developmental genetics is that evolution employs a relatively small number of signaling pathways to control a wide range of embryological processes. The present work extends this theme by linking the mechanisms responsible for palate, ventricular septum and neural tube closure. Although these processes occur within

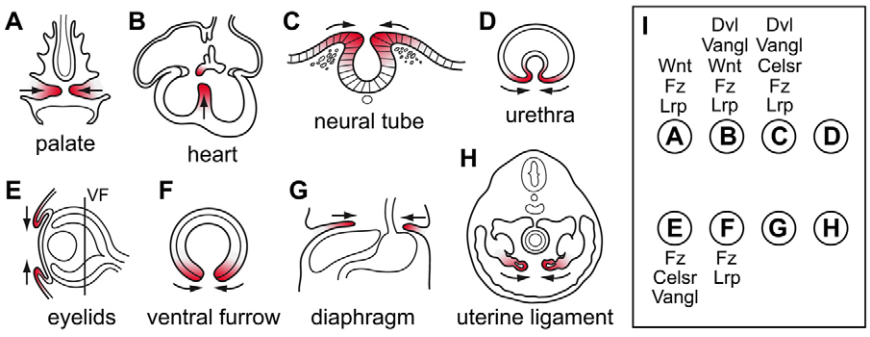

Fig. 7. Diverse tissue closure processes in mammalian development, and the involvement of PCP and canonical Wnt signaling genes. (**A-H**) Eight tissue closure processes are shown. The plane of section is shown in E for the ventral furrow (VF) in the eye (F). The closing tissue is highlighted in red, and arrows indicate the direction of movement. (**I**) The general classes of PCP and canonical Wnt signaling genes that are involved in each closure process depicted in A-H are listed adjacent to the corresponding letters; in some cases, defects are only seen when more than one redundant or partially redundant gene is mutated.

different anatomical contexts, we can rationalize the use of shared signaling pathways by noting that each involves directional tissue movements followed by tissue fusion. It is apparent that a number of other embryological processes conform to this pattern, including closure of the ventral urethra, the eyelids, the ventral furrow in the eye, the diaphragm and the uterine ligament (Fig. 7A-H). Congenital defects in several of these processes are relatively common, with frequencies of 1/250, 1/3000 and 1/30,000 for hypospadia, congenital diaphragmatic hernia and ocular coloboma, respectively (Bielinska et al., 2007; Utsch et al., 2004; Vogt et al., 2006). Although it is unknown whether frizzled signaling plays a role in this second set of closure processes, the essential roles played by frizzled proteins and other functionally interacting signaling components in the palate, heart, neural tube and eye (Fig. 7I) suggest this possibility (Pinson et al., 2000; Barbosa et al., 2003; Curtin et al., 2003; Etheridge et al., 2008; He et al., 2008; Kibar et al., 2001; Murdoch et al., 2001; Schleiffarth et al., 2007; Wang et al., 2006; Wang et al., 2005; Wang and Nathans, 2007; Song et al., 2009; Song et al., 2010).

Implications of redundancy and near-threshold action in frizzled signaling

The substantial redundancy of *Fz1* and *Fz2* reflects their high degree of sequence similarity and largely overlapping patterns of expression. Partial redundancy has also been observed among other mammalian PCP and canonical signaling components, including Fz3/Fz6 (Wang et al., 2006), Vangl1/Vangl2 (Torban et al., 2008), Dvl1/Dvl2/Dvl3 (Etheridge et al., 2008; Wang et al., 2006; Wang et al., 2005) and Lrp5/Lrp6 (Ye et al., 2009). Partial redundancy could reflect gene dosage effects. For example, progressively lowering the level of Fz1 and Fz2 signaling by eliminating only Fz2 leads to 50% penetrant clefting, whereas eliminating both Fz1 and Fz2 leads to 100% penetrant clefting. Similarly, Vangl2 signaling appears to be only marginally above the threshold for normal development, as heterozygosity for the *Lp* allele causes tail curling and reduced fertility and sensitizes the embryo to inner ear, cardiac and neural tube defects in the background of heterozygous or homozygous loss of function for *Ptk7*, *Dvl2*, *Dv13*, *Fz1* and *Fz2* (Etheridge et al., 2008; Lu et al., 2004; Wang et al., 2006; Wang et al., 2005) (this work).

Partial redundancy and near-threshold levels of gene function have several implications for the genetics of palate, ventricular septum and neural tube closure in humans. First, mutations in some genes that play an essential role in these processes might only rarely, if ever, be associated with disease because they are masked by redundancy; second, for other genes, loss-of-function mutations might be associated with disease, but only in combination with additional genetic and/or environmental variations; and third, patients with combinations of congenital tissue closure anomalies – for example, cleft palate and congenital heart disease (Barbosa et al., 2003; Geis et al., 1981; Milerad et al., 1997) – might carry mutations in genes that contribute to multiple closure processes. The recent discovery of rare sequence variants in *VANGL1* in patients with neural tube defects might relate to the first two points (Kibar et al., 2009; Kibar et al., 2007b). These considerations suggest that large-scale sequencing of DNA from individuals with tissue closure anomalies might reveal associated genetic variations, either singly or in combination, in a variety of PCP and/or canonical Wnt signaling genes. Together with experiments in animal models, such analyses will lead to a better understanding of the gene networks that mediate tissue closure events in embryonic development.

Acknowledgements
We thank Shizuka Aoki, Tudor Badea, Hao Chang, David Huso, Se-Jin Lee, Janet Rossant, Hao Wu and Xin Ye for advice, materials and/or comments on the manuscript. Supported by the Howard Hughes Medical Institute. Deposited in PMC for release after 6 months.

Competing interests statement
The authors declare no competing financial interests.

Supplementary material
Supplementary material for this article is available at
http://dev.biologists.org/lookup/suppl/doi:10.1242/dev.052001/-/DC1

References
Bakalyar, H. A. and Reed, R. R. (1990). Identification of a specialized adenylyl cyclase that may mediate odorant detection. *Science* **250**, 1403-1406.
Barbosa, M. M., Rocha, C. M., Katina, T., Caldas, M., Codorniz, A. and Medeiros, C. (2003). Prevalence of congenital heart diseases in oral cleft patients. *Pediatr. Cardiol.* **24**, 369-374.
Belluscio, L., Gold, G. H., Nemes, A. and Axel, R. (1998). Mice deficient in G(olf) are anosmic. *Neuron* **20**, 69-81.
Bielinska, M., Jay, P. Y., Erlich, J. M., Mannisto, S., Urban, Z., Heikinheimo, M. and Wilson, D. B. (2007). Molecular genetics of congenital diaphragmatic defects. *Ann. Med.* **39**, 261-274.
Centers for Disease Control (1997). Surveillance summaries and temporal trends in the incidence of birth defects – United States. *Morb. Mortal. Wkly. Rep.* **46**, 1171-1176.
Chan, S. D., Karpf, D. B., Fowlkes, M. E., Hooks, M., Bradley, M. S., Vuong, V., Bambino, T., Liu, M. Y., Arnaud, C. D., Strewler, G. J. et al. (1992). Two homologs of the Drosophila polarity gene frizzled (fz) are widely expressed in mammalian tissues. *J. Biol. Chem.* **267**, 25202-25207.
Chen, J., Rattner, A. and Nathans, J. (2005). The rod photoreceptor-specific nuclear receptor Nr2e3 represses transcription of multiple cone-specific genes. *J. Neurosci.* **25**, 118-129.
Cohen, E. D., Tian, Y. and Morrisey, E. E. (2008). Wnt signaling: an essential regulator of cardiovascular differentiation, morphogenesis and progenitor self-renewal. *Development* **135**, 789-798.
Copp, A. J. and Greene, N. D. (2010). Genetics and development of neural tube defects. *J. Pathol.* **220**, 217-230.
Curtin, J. A., Quint, E., Tsipouri, V., Arkell, R. M., Cattanach, B., Copp, A. J., Henderson, D. J., Spurr, N., Stanier, P., Fisher, E. M. et al. (2003). Mutation of Celsr1 disrupts planar polarity of inner ear hair cells and causes severe neural tube defects in the mouse. *Curr. Biol.* **13**, 1129-1133.
Deans, M. R., Antic, D., Suyama, K., Scott, M. P., Axelrod, J. D. and Goodrich, L. V. (2007). Asymmetric distribution of prickle-like 2 reveals an early underlying polarization of vestibular sensory epithelia in the inner ear. *J. Neurosci.* **27**, 3139-3147.
Etheridge, S. L., Ray, S., Li, S., Hamblet, N. S., Lijam, N., Tsang, M., Greer, J., Kardos, N., Wang, J., Sussman, D. J. et al. (2008). Murine dishevelled 3 functions in redundant pathways with dishevelled 1 and 2 in normal cardiac outflow tract, cochlea, and neural tube development. *PLoS Genet.* **4**, e1000259.
Geis, N., Seto, B., Bartoshesky, L., Lewis, M. B. and Pashayan, H. M. (1981). The prevalence of congenital heart disease among the population of a metropolitan cleft lip and palate clinic. *Cleft Palate J.* **18**, 19-23.
Genisca, A. E., Frias, J. L., Broussard, C. S., Honein, M. A., Lammer, E. J., Moore, C. A., Shaw, G. M., Murray, J. C., Yang, W. and Rasmussen, S. A. (2009). Orofacial clefts in the National Birth Defects Prevention Study, 1997-2004. *Am. J. Med. Genet. A* **149A**, 1149-1158.
Gong, S. G. and Eulenberg, R. L. (2001). Palatal development in Twirler mice. *Cleft Palate Craniofac. J.* **38**, 622-628.
Grinberg, I. and Millen, K. J. (2005). The ZIC gene family in development and disease. *Clin. Genet.* **67**, 290-296.
Gritli-Linde, A. (2007). Molecular control of secondary palate development. *Dev. Biol.* **301**, 309-326.
Hayashi, S., Lewis, P., Pevny, L. and McMahon, A. P. (2002). Efficient gene modulation in mouse epiblast using a Sox2Cre transgenic mouse strain. *Gene Expr. Patterns* **2**, 93-97.
He, F., Xiong, W., Yu, X., Espinoza-Lewis, R., Liu, C., Gu, S., Nishita, M., Suzuki, K., Yamada, G., Minami, Y. et al. (2008). Wnt5a regulates directional cell migration and cell proliferation via Ror2-mediated noncanonical pathway in mammalian palate development. *Development* **135**, 3871-3879.
Henderson, D. J., Phillips, H. M. and Chaudhry, B. (2006). Vang-like 2 and noncanonical Wnt signaling in outflow tract development. *Trends Cardiovasc. Med.* **16**, 38-45.
Henderson, D. J., Conway, S. J., Greene, N. D. E., Gerrelli, D., Murdoch, J. N., Anderson, R. H. and Copp, A. J. (2009). Cardiovascular defects associated with abnormalities in midline development in the Loop-tail mouse mutant. *Circ. Res.* **89**, 6-12.

Hoffman, J. I. and Kaplan, S. (2002). The incidence of congenital heart disease. *J. Am. Coll. Cardiol.* **39**, 1890-1900.
Hogan, B., Costantini, F. and Lacy, E. (1994). *Manipulating the Mouse Embryo*, 2nd edn, pp. 379-380. Cold Spring Harbor, NY: Cold Spring Harbor Laboratory Press.
Inoue, T., Ota, M., Mikoshiba, K. and Aruga, J. (2007). Zic2 and Zic3 synergistically control neurulation and segmentation of paraxial mesoderm in mouse embryo. *Dev. Biol.* **306**, 669-684.
Jugessur, A. and Murray, J. C. (2005). Orofacial clefting: recent insights into a complex trait. *Curr. Opin. Genet. Dev.* **15**, 270-278.
Juriloff, D. M. and Harris, M. J. (2008). Mouse genetic models of cleft lip with or without cleft palate. *Birth Defects Res. A Clin. Mol. Teratol.* **82**, 63-77.
Juriloff, D. M., Harris, M. J., McMahon, A. P., Carroll, T. J. and Lidral, A. C. (2006). Wnt9b is the mutated gene involved in multifactorial nonsyndromic cleft lip with or without cleft palate in A/WySn mice, as confirmed by a genetic complementation test. *Birth Defects Res. A Clin. Mol. Teratol.* **76**, 574-579.
Keller, R. (2002). Shaping the vertebrate body plan by polarized embryonic cell movements. *Science* **298**, 1950-1954.
Kibar, Z., Vogan, K. J., Groulx, N., Justice, M. J., Underhill, D. A. and Gros, P. (2001). Ltap, a mammalian homolog of Drosophila Strabismus/Van Gogh, is altered in the mouse neural tube mutant Loop-tail. *Nat. Genet.* **28**, 251-255.
Kibar, Z., Capra, V. and Gros, P. (2007a). Toward understanding the genetic basis of neural tube defects. *Clin. Genet.* **71**, 295-310.
Kibar, Z., Torban, E., McDearmid, J. R., Reynolds, A., Berghout, J., Mathieu, M., Kirillova, I., De Marco, P., Merello, E., Hayes, J. M. et al. (2007b). Mutations in VANGL1 associated with neural-tube defects. *New Engl. J. Med.* **356**, 1432-1437.
Kibar, Z., Bosoi, C. M., Kooistra, M., Salem, S., Finnell, R. H., De Marco, P., Merello, E., Bassuk, A. G., Capra, V. and Gros, P. (2009). Novel mutations in VANGL1 in neural tube defects. *Hum. Mutat.* **30**, E706-E715.
Lee, J. M., Kim, J. Y., Cho, K. W., Lee, M. J., Cho, S. W., Kwak, S., Cai, J. and Jung, H. S. (2008). Wnt11/Fgfr1b cross-talk modulates the fate of cells in palate development. *Dev. Biol.* **314**, 341-350.
Liu, C. and Nathans, J. (2008). An essential role for frizzled5 in mammalian ocular development. *Development* **135**, 3567-3576.
Lu, X., Borchers, A. G., Jolicoeur, C., Rayburn, H., Baker, J. C. and Tessier-Lavigne, M. (2004). PTK7/CCK-4 is a novel regulator of planar cell polarity in vertebrates. *Nature* **430**, 93-98.
Milerad, J., Larson, O., Ph, D. D., Hagberg, C. and Ideberg, M. (1997). Associated malformations in infants with cleft lip and palate: a prospective, population-based study. *Pediatrics* **100**, 180-186.
Montcouquiol, M., Rachel, R. A., Lanford, P. J., Copeland, N. G., Jenkins, N. A. and Kelley, M. W. (2003). Identification of Vangl2 and Scrb1 as planar polarity genes in mammals. *Nature* **423**, 173-177.
Moon, A. (2008). Mouse models of congenital cardiovascular disease. *Curr. Top. Dev. Biol.* **84**, 171-248.
Murdoch, J. N., Doudney, K., Paternotte, C., Copp, A. J. and Stanier, P. (2001). Severe neural tube defects in the loop-tail mouse result from mutation of Lpp1, a novel gene involved in floor plate specification. *Hum. Mol. Genet.* **10**, 2593-2601.
New York State Department of Health (2001). Congenital malformations registry – summary report. Section V: Comparison of selected malformation prevalence with other birth defects registries. http://www.health.state.ny.us/diseases/congenital_malformations/1998_2001/section5.htm.
Niemann, S., Zhao, C., Pascu, F., Stahl, U., Aulepp, U., Niswander, L., Weber, J. L. and Muller, U. (2004). Homozygous WNT3 mutation causes tetra-amelia in a large consanguineous family. *Am. J. Hum. Genet.* **74**, 558-563.
Phillips, H. M., Murdoch, J. N., Chaudhry, B., Copp, A. J. and Henderson, D. J. (2005). Vangl2 acts via RhoA signaling to regulate polarized cell movements during development of the proximal outflow tract. *Circ. Res.* **96**, 292-299.
Pinson, K. I., Brennan, J., Monkley, S., Avery, B. J. and Skarnes, W. C. (2000). An LDL-receptor-related protein mediates Wnt signalling in mice. *Nature* **407**, 535-538.
Salic, A. and Mitchison, T. J. (2008). A chemical method for fast and sensitive detection of DNA synthesis in vivo. *Proc. Natl. Acad. Sci. USA* **105**, 2415-2420.
Schleiffarth, J. R., Person, A. D., Martinsen, B. J., Sukovich, D. J., Neumann, A., Baker, C. V., Lohr, J. L., Cornfield, D. N., Ekker, S. C. and Petryk, A. (2007). Wnt5a is required for cardiac outflow tract septation in mice. *Pediatr. Res.* **61**, 386-391.
Seifert, J. R. and Mlodzik, M. (2007). Frizzled/PCP signalling: a conserved mechanism regulating cell polarity and directed motility. *Nat. Rev. Genet.* **8**, 126-138.
Shepard, T. H., Fantel, A. G. and Fitzsimmons, J. (1989). Congenital defect rates among spontaneous abortuses: twenty years of monitoring. *Teratology* **39**, 325-331.
Simons, M., Gloy, J., Ganner, A., Bullerkotte, A., Bashkurov, M., Krönig, C., Schermer, B., Benzing, T., Cabello, O. A., Jenny, A. et al. (2005). Inversin, the gene product mutated in nephronophthisis type II, functions as a molecular switch between Wnt signaling pathways. *Nat. Genet.* **37**, 537-543.
Song, L., Li, Y., Wang, K., Wang, Y. Z., Molotkov, A., Gao, L., Zhao, T., Yamagami, T., Wang, Y., Gan, Q. et al. (2009). Lrp6-mediated canonical Wnt signaling is required for lip formation and fusion. *Development* **136**, 3161-3171.
Song, L., Li, Y., Wang, K. and Zhou, C. J. (2010). Cardiac neural crest and outflow tract defects in Lrp6 mutant mice. *Dev. Dyn.* **239**, 200-210.
Torban, E., Patenaude, A. M., Leclerc, S., Rakowiecki, S., Gauthier, S., Andelfinger, G., Epstein, D. J. and Gros, P. (2008). Genetic interaction between members of the Vangl family causes neural tube defects in mice. *Proc. Natl. Acad. Sci. USA* **105**, 3449-3454.
Tudela, C., Formoso, M. A., Martinez, T., Perez, R., Aparicio, M., Maestro, C., Del Rio, A., Martinez, E., Ferguson, M. and Martinez-Alvarez, C. (2002). TGF-beta3 is required for the adhesion and intercalation of medial edge epithelial cells during palate fusion. *Int. J. Dev. Biol.* **46**, 333-336.
Utsch, B., Albers, N. and Ludwig, M. (2004). Genetic and molecular aspects of hypospadias. *Eur. J. Pediatr. Surg.* **14**, 297-302.
van Gijn, M. E., Blankesteijn, W. M., Smits, J. F., Hierck, B. and Gittenberger-de Groot, A. C. (2001). Frizzled 2 is transiently expressed in neural crest-containing areas during development of the heart and great arteries in the mouse. *Anat. Embryol.* **203**, 185-192.
Veeman, M. T., Axelrod, J. D. and Moon, R. T. (2003). A second canon. Functions and mechanisms of beta-catenin-independent Wnt signaling. *Dev. Cell* **5**, 367-377.
Vogt, G., Szunyogh, M. and Czeizel, A. E. (2006). Birth characteristics of different ocular congenital abnormalities in hungary. *Ophthalmic Epidemiol.* **13**, 159-166.
Wallingford, J. B., Fraser, S. E. and Harland, R. M. (2002). Convergent extension: the molecular control of polarized cell movement during embryonic development. *Dev. Cell* **2**, 695-706.
Wang, J., Mark, S., Zhang, X., Qian, D., Yoo, S. J., Radde-Gallwitz, K., Zhang, Y., Lin, X., Collazo, A., Wynshaw-Boris, A. et al. (2005). Regulation of polarized extension and planar cell polarity in the cochlea by the vertebrate PCP pathway. *Nat. Genet.* **37**, 980-985.
Wang, J., Hamblet, N. S., Mark, S., Dickinson, M. E., Brinkman, B. C., Segil, N., Fraser, S. E., Chen, P., Wallingford, J. B. and Wynshaw-Boris, A. (2006). Dishevelled genes mediate a conserved mammalian PCP pathway to regulate convergent extension during neurulation. *Development* **133**, 1767-1778.
Wang, S. S., Tsai, R. Y. and Reed, R. R. (1997). The characterization of the Olf-1/EBF-like transcription factor family: implications in olfactory gene regulation and neuronal development. *J. Neurosci.* **17**, 4159-4169.
Wang, Y. and Nathans, J. (2007). Tissue/planar cell polarity in vertebrates: new insights and new questions. *Development* **134**, 647-658.
Wang, Y., Macke, J. P., Abella, B. S., Andreasson, K., Worley, P., Gilbert, D. J., Copeland, N. G., Jenkins, N. A. and Nathans, J. (1996). A large family of putative transmembrane receptors homologous to the product of the Drosophila tissue polarity gene frizzled. *J. Biol. Chem.* **271**, 4468-4476.
Wang, Y., Guo, N. and Nathans, J. (2006). The role of Frizzled3 and Frizzled6 in neural tube closure and in the planar polarity of inner-ear sensory hair cells. *J. Neurosci.* **26**, 2147-2156.
Warner, D. R., Smith, H. S., Webb, C. L., Greene, R. M. and Pisano, M. M. (2009). Expression of Wnts in the developing murine secondary palate. *Int. J. Dev. Biol.* **53**, 1105-1112.
Xu, Q., Wang, Y., Dabdoub, A., Smallwood, P. M., Williams, J., Woods, C., Kelley, M. W., Jiang, L., Tasman, W., Zhang, K. et al. (2004). Vascular development in the retina and inner ear: control by Norrin and Frizzled-4, a high-affinity ligand-receptor pair. *Cell* **116**, 883-895.
Ye, X., Wang, Y., Cahill, H., Yu, M., Badea, T. C., Smallwood, P. M., Peachey, N. S. and Nathans, J. (2009). Norrin, frizzled-4, and Lrp5 signaling in endothelial cells controls a genetic program for retinal vascularization. *Cell* **139**, 285-298.
Zhao, H. and Reed, R. R. (2001). X inactivation of the OCNC1 channel gene reveals a role for activity-dependent competition in the olfactory system. *Cell* **104**, 651-660.
Zhou, W., Lin, L., Majumdar, A., Li, X., Zhang, X., Liu, W., Etheridge, L., Shi, Y., Martin, J., Van de Ven, W. et al. (2007). Modulation of morphogenesis by noncanonical Wnt signaling requires ATF/CREB family-mediated transcriptional activation of TGFβ2. *Nat. Genet.* **39**, 1225-1234.